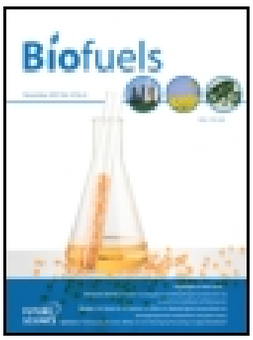

Biofuels

ISSN: 1759-7269 (Print) 1759-7277 (Online) Journal homepage: http://www.tandfonline.com/loi/tbfu20

Effect of exhaust gas recirculation rate on performance, emission and combustion characteristics of a common-rail diesel engine fuelled with n-butanol–diesel blends

Venkatesh Tavareppa Lamani, Ajay Kumar Yadav & Kumar Narayanappa Gottekere

To cite this article: Venkatesh Tavareppa Lamani, Ajay Kumar Yadav & Kumar Narayanappa Gottekere (2017): Effect of exhaust gas recirculation rate on performance, emission and combustion characteristics of a common-rail diesel engine fuelled with n-butanol–diesel blends, Biofuels, DOI: 10.1080/17597269.2017.1369631

To link to this article: http://dx.doi.org/10.1080/17597269.2017.1369631

Published online: 11 Sep 2017.

BIOFUELS, 2017
https://doi.org/10.1080/17597269.2017.1369631

Taylor & Francis
Taylor & Francis Group

Effect of exhaust gas recirculation rate on performance, emission and combustion characteristics of a common-rail diesel engine fuelled with n-butanol–diesel blends

Venkatesh Tavareppa Lamani, Ajay Kumar Yadav and Kumar Narayanappa Gottekere

Department of Mechanical Engineering, National Institute of Technology Karnataka, Surathkal, Mangalore–575 025, India

ABSTRACT

Increasing fears of fossil fuel attenuation and tough emission protocols compel the research community to explore alternative renewable fuels for diesel engines. Butanol is desirable among renewable fuels due to its properties favorable to diesel engines. This study focused on the suitability of exhaust gas recirculation (EGR) and optimum injection timing on the performance, combustion and exhaust emission characteristics of common-rail direct-injection (CRDI) engine fueled with n-butanol-blended diesel using experimental and computational fluid dynamics (CFD) simulation. Various EGR rates and injection timings are considered for different butanol–diesel blends (0, 10, 20 and 30%). Obtained simulation results are validated with experimental data and found to be in good agreement. For all EGR rates and blends, nitrogen oxide (NO) emission is reduced drastically, whereas carbon monoxide (CO) and soot emissions are decreased moderately, with increase in n-butanol–diesel blends. The CO and soot emissions increase with EGR rate due to oxygen deficiency as well. Brake thermal efficiency is reduced by approximately 1% for neat diesel (Bu0) with increase in EGR rates. Soot emission for Bu30 (15 ° Before top dead centre (BTDC) is decreased by 23, 25, 24 and 26% for 0, 10, 20 and 30% EGR rates, respectively, compared to Bu0 (12° BTDC).

ARTICLE HISTORY
Received 8 April 2017
Accepted 3 August 2017

KEYWORDS
CRDI; CFD; exhaust gas recirculation; combustion analysis; n-butanol; emission

Nomenclature

Bu	Butanol
CRDI	Common-rail direct injection
D_t	Diffusion coefficient
$\dot{\breve{E}}_{Fu}^{F\rightarrow M}$	Unmixed fuel source term
$\dot{\breve{E}}_{O_2}^{A\rightarrow M}$	Unmixed oxygen source term
M_{Fu}	Molar mass of fuel
R	Universal gas constant
S_c and S_{ct}	Laminar and turbulent Schmidt numbers
$\overline{S}_{NO}$	Mean nitric oxide source term
$\tilde{u}$	Density-weighted average velocity
$\overline{\dot{\omega}}_x$	Average combustion source term
ζ	Transformed coordinate system
$\overline{\rho}^u\|_u$	Density of the unburned gases
ε	Dissipation rate
ϕ	Equivalence ratio
ϕ_s	Soot mass fraction
μ	Dynamic viscosity
τ_d	Ignition delay
$\overline{\rho}$	Reynolds averaged fuel density
$\breve{Y}_{NO}$	Mean mass fraction of NO_x
x_i	Cartesian coordinates
M_{NO}	Molar mass
$\frac{dc_{NO\ prompt}}{dt}$	Prompt mechanisms
$\frac{dc_{NO\ thermal}}{dt}$	Thermal mechanisms
μ_t	Turbulent viscosity
$\breve{Y}_x$	Averaged mass fraction of species x
M^M	Mean molar mass of the gases in the mixed area
M_{Fu}	Molar mass of fuel
$M_{air+\ EGR}$	Mean molar mass of the unmixed air + EGR gases
$\overline{\rho}$	Mean density
$\breve{Y}_{O_2}^{\infty}$	Oxygen mass fraction
τ_m	Mixing time
$\breve{Y}_{TO_2}$	Oxygen tracer
$\breve{Y}_{TFu}$	Fuel tracer

Introduction

With the fossil fuel crisis and rigid levied emission guidelines owing to environmental deprivation, finding a renewable alternative fuel has become a challenging task for researchers. Biofuels are renewable, sustainable and environmentally acceptable energy sources, which can be extracted from edible as well as agricultural waste such as corn, sugarcane, starch, molasses, wheat straw, corn stover and other cellulose. Butanol is competent among biofuels due to its higher volumetric energy content, excellent blending stability, better miscibility, higher cetane number, lower heat of vaporization, and mildly corrosive and lower auto-ignition temperature compared to ethanol and methanol.

CONTACT Ajay Kumar Yadav ajayyadav.aba@rediffmail.com

Hence, fewer ignition problems occur with butanol compared to ethanol and methanol [1–4]. Zheng et al. [5] reported that crude glycerol can be converted to biofuel comprising mainly butanol. Further, the presence of an additional oxygen atom in alcohol results in efficient combustion with an increase in combustion efficiency and decrease in emissions, mainly of soot, CO and hydrocarbons (HC) [6–8].

Rakopoulos et al. [9] experimentally observed the performance and tailpipe emissions of a direct-injection engine fuelled with butanol–diesel blends. Their study revealed that n-butanol is a promising substitute fuel for compression-ignition (CI) engines. The effects of fuel properties on engine performance and emission features of a diesel engine operated with n-butanol–diesel blends were examined by Lujaji et al. [10]. They showed that tailpipe emissions such as CO and soot are reduced for n-butanol in comparison to diesel.

Experimental investigation on a naturally aspirated, four-stroke, unmodified CI engine was conducted by Dogan et al. [11]. They observed a reduction in nitrogen oxide, soot and CO emissions, while unburned HC emission was increased when the engine was operated with higher n-butanol diesel blends. Rakopoulos et al. [12] conducted an experimental investigation on a four-stroke, variable-speed, constant-load high-speed diesel engine fuelled with n-butanol–diesel blends. They reported a drastic drop in NO_x and CO emission, with a marginal increase in HC for higher blends. Butanol was also experimented on with different vegetable oils (canola–hazelnut–cottonseed oil [CHC] and neat sunflower–corn–soybean oil [SCS]) in diesel engines, and found to cause an improvement in cold-flow properties of vegetable oils [13].

Several studies estimated the effects of EGR rates in a diesel engine fuelled with n-butanol–diesel blends. Studies on the effect of n-butanol–diesel blends and low-temperature combustion reported by Valentino et al. [14] and Chen et al. [15] show an upsurge in in-cylinder pressure due to a faster burning rate and longer ignition delay. Experiments conducted by Yao et al. [16] and Kumar et al. [17] on engines operated with EGR reveal the reduction of NO_x and smoke emissions.

From the available literature, it can be seen that studies of biobutanol–diesel blends with optimum injection timing are not available. Based on the fuel, injection time should be optimized in terms of performance of the engine. Comparing the effect of EGR on emission characteristics and performance of an engine at optimum injection timings for blends and neat diesel is greatly justified. Further investigation of the effect of biobutanol–diesel blends on a CRDI engine with CFD simulation is scant. CFD simulation offers the prospect to achieve a deeper insight into in-cylinder combustion. In the present study, comprehensive experimental and CFD analyses on performance, combustion and emission characteristics of a twin-cylinder common-rail direct-injection engine using n-butanol diesel blends are carried out. In the case of butanol (C_4H_9OH), a fuel-bound oxygen atom is present in the fuel and enhances the combustion. In this study, we explore the details of variations in the engine performance, emissions and combustion characteristics for various n-butanol diesel blends, EGR rates and injection timings. The EGR technique is employed in both experiments and in the CFD simulation. EGR is a promising technique to mitigate the NO emission significantly. In-cylinder pressure and engine-out emissions of soot, NO and CO are measured experimentally.

Table 1. Properties of diesel and n-butanol.

Fuel properties	Diesel fuel	n-butanol	Bu10	Bu20	Bu30
Density at 20 °C (kg/m^3)	837	810	834.3	831.6	828.9
Lower calorific value (MJ/kg)	43	33.1	42.01	41.02	40.03
Kinematic viscosity at 40 °C (mm^2/s)	2.6	3.6	2.7	2.8	2.9
Latent heat of evaporation (kJ/kg)	250	585	283.5	317	350.5
Cetane number	47	25	42	37	32
Oxygen (wt.%)	0	21.6	2.09	4.2	6.3
Stoichiometric air–fuel ratio	15	11.2	14.62	14.24	13.86

Materials and methods

Fuel properties and combustion strategy

In the present investigation, n-butanol–diesel blends are considered for numerical and experimental studies. The n-butanol is blended with neat diesel to obtain different blends from 0 to 30% by volume. Bu0, Bu10, Bu20 and Bu30 represent 0, 10, 20 and 30% n-butanol in neat diesel, respectively. The cetane number (CN) of biobutanol–diesel blended fuel is a function of biobutanol content in the diesel fuel; hence, the higher the butanol blend, the lower the the cetane number. Therefore, in the present study a range of butanol–diesel blends up to 30% are considered. The basic physical properties of n-butanol and neat diesel employed in this investigation are compared in Table 1 [9], and the range of experimental parameters are listed in Table 2.

Experimental set-up

A schematic diagram and representation of the experimental facility are shown in Figure 1(a,b). A twin-cylinder, CRDI engine with an open electronic control unit

Table 2. Range of simulation parameters.

Parameters	Range
Blend (% of n-butanol)	0, 10, 20, 30
EGR (%) experimental	0, 10, 20
EGR (%) simulation	0, 10, 20, 30
Injection timings	9°, 12°, 15° and 18°

(ECU) developed by NIRA Control AB, is used to study the engine performance, emission and combustion characteristics. The specifications of the engine are listed in Table 3.

The fuel from the tank is supplied to the accumulator (common rail) by a high-pressure fuel pump at constant injection pressure of 100 MPa. Common-rail pressure is maintained by a pressure control valve (PCV) and the required fuel supplied to the injector is controlled by a solenoid valve. Operating parameters (injection timing, EGR, injection pressure) of the engine are controlled by the open ECU. Pressure versus crank angle data is measured using a piezoelectric-based pressure transducer. The signal of cylinder pressure is acquired at every 1° crank angle for 100 cycles, and the average value of 100 cycles is considered for combustion analysis. The pressure signal is fed into the NI USB-6210 DAQ, then to a data acquisition card linked to the computer.

EGR is activated by ECU with a vacuum pump, solenoid valve and vacuum modulator. The required EGR value is set with an ECU map, that monitors the vacuum pump to maintain the required vacuum, and the solenoid valve operates accordingly. Further, engine tailpipe emissions (HC, CO, NO, CO_2 and O_2) are measured by an exhaust gas analyzer (AVL 444) with diesel probe. Soot emission is measured with an opacity meter (AVL 415SE). Details of the engine instrumentation are presented in Tables 4 and 5.

Table 3. Engine specifications.

Make	Mahindra Maximmo
Number of cylinders	2
Bore × Stroke (mm)	83 × 84
Connecting rod length (mm)	141
Swept volume (cm^3)	909
Compression ratio	18.5
Injection type	Common rail
Injection pressure (MPa)	100

Error analysis

Assessment of uncertainties and error is necessary while conducting any experimental study. Uncertainties may appear for numerous reasons, such as environmental conditions, calibration, observation,

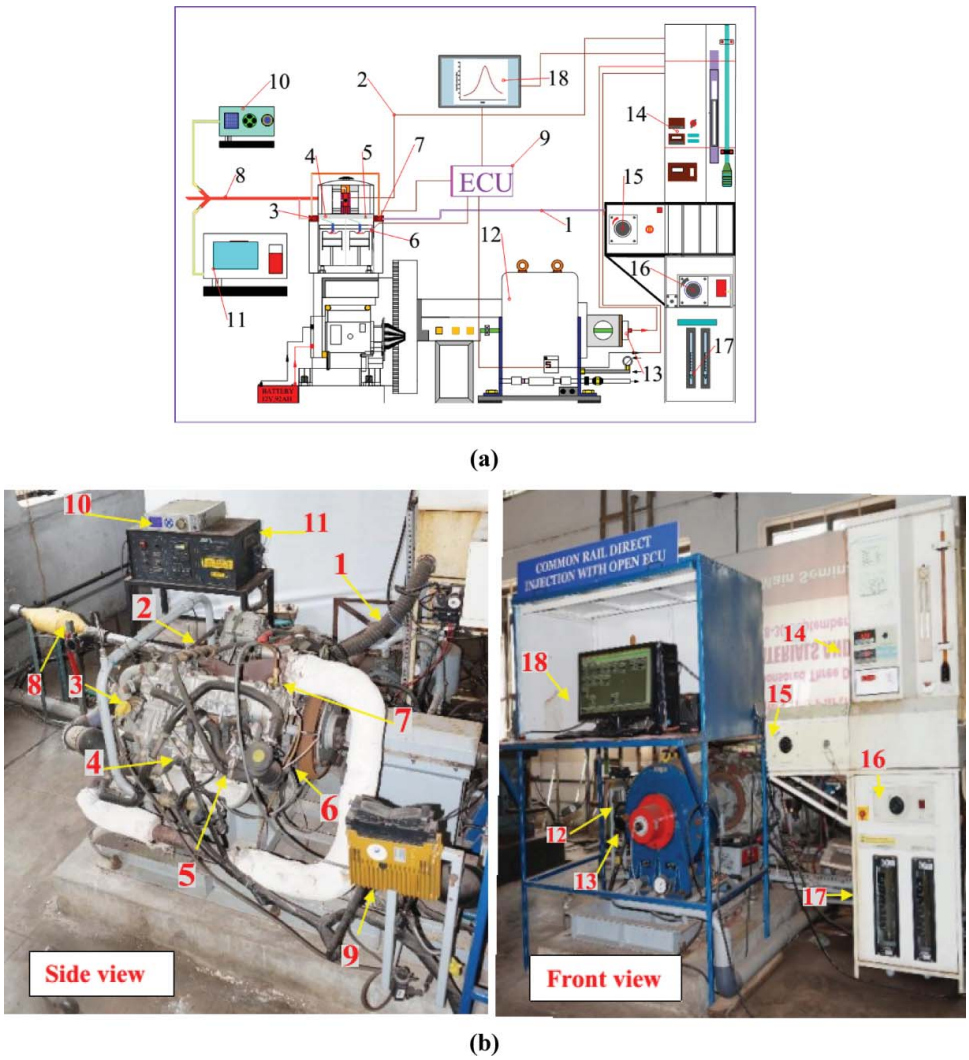

Figure 1. (a) Schematic diagram, and (b) experimental facility.

Table 4. Details of the engine instrumentation.

Instrument	Functional use	Measuring technique
Saj test – eddy dynamometer	Load	Load cell
PCB piezotronics, pressure transducer	Pressure	Piezo-electric sensor
Piezo Charge Amplifier	A/D converter	Piezo-electric sensor
Angle Encoder	Crank angle	Magnetic pickup type
AVL Di-gas 444 exhaust gas analyzer	NO_x	Chemi-luminescence detector (CLD)
	CO	Non-dispersive infra-red (NDIR)
	Hydrocarbon (HC) emissions	Flame ionization detector (FID)
AVL 415SE	Soot	Opacity

instrument selection and incorrect reading. Error analysis quantifies the accuracy of the experiments being performed. The uncertainties of dependent parameters such as brake power and fuel consumption are computed by a partial differentiation method using the uncertainty percentages of various instruments as shown in Table 5 [17]. The uncertainties for independent parameters were found by calculating the mean, standard deviation and standard error for the repeated set of 20 readings. The total uncertainty of the experimental investigation is as follows:

Square root of {(uncertainty of CO)^2 + (uncertainty of NO)^2 + (uncertainty of soot)^2 + (uncertainty of load)^2 + (uncertainty of speed)^2 + (uncertainty of time)^2 + (uncertainty of brake power)^2 + (uncertainty of fuel consumption)^2 + (uncertainty of brake thermal efficiency)^2 + (uncertainty of cylinder pressure)^2 + (uncertainty of crank angle)^2 + (uncertainty of manometer)^2}.

= Square root of {$(0.1)^2$ +$(0.6)^2$ + $(0.1)^2$ + $(1.3)^2$ + $(0.1)^2$ + $(0.2)^2$ + $(0.8)^2$ + $(0.2)^2$ + $(0.8)^2$ + $(0.9)^2$ + $(0.1)^2$ + $(0.2)^2$ }.

±2.076%.

CFD code and meshing of geometry

The AVL ESE CFD tool is used for engine geometric modelling, computational meshing and simulation for the present study.

The injector, with seven holes, is located centrally on the top of the piston; hence, the 51.43° sector is chosen for the simulation. The three-dimensional computational domain of a sector at a different position with reference to Top dead centre (TDC) is shown in Figure 2. In order to reduce the computational time, a high-pressure cycle is considered. Simulation is started and ended at inlet valve close and exhaust valve open position, respectively. A grid independence test has been carried out to obtain the optimum grid size, as shown in Figure 3. Simulation is carried out by a 64 GB RAM 32 core workstation with parallel processing. The results were checked for peak pressure and computational time for various grid sizes. It was observed that the considered parameters are invariant with change in the total number of grids at/after 3×10^5. Boundary conditions and models employed in the simulation are listed in Tables 6 and 7, respectively.

Table 5. Operating range with percentage of uncertainties of instruments used during experiments.

Instrument (%)	Measured quantity	Range	Uncertainty
Dynamometer	Load	0–50 kg	0.1
AVL Di-Gas 444 analyzer	NO_x	0–5000 ppm	0.1
	CO	0–10 vol.%	0.1
Smoke opacimeter	Smoke opacity	0–100%	1.7
Speed measuring unit	Engine speed	0–9999rpm	0.1
Pressure transducer	Cylinder pressure	0–345 bar	0.1
Crank angle encoder	Crank angle	0–360°	0.2

Governing equations

A general transport equation for chemical species is given by [18]:

$$\frac{\partial(\overline{\rho}Y_x)}{\partial t} + \frac{\partial(\overline{u}_i\overline{\rho}Y_x)}{\partial x_i} = \frac{\partial}{\partial x_i}\left(\left(\frac{\mu}{S_c} + \frac{\mu}{S_{ct}}\right)\frac{\partial Y_x}{\partial x_i}\right) + \overline{\dot{\omega}}_x \quad (1)$$

Fuel transport equations for unburned and burned fuel mass fractions are given by Colin and Benkenida [19]:

$$\frac{\partial(\overline{\rho}Y^u_{Fu})}{\partial t} + \frac{\partial(\overline{\rho}u_i\overline{\rho}Y^u_{Fu})}{\partial x_i} = \frac{\partial}{\partial x_i}\left(\left(\frac{\mu}{S_c} + \frac{\mu_t}{S_{ct}}\right)\frac{\partial Y^u_{Fu}}{\partial x_i}\right) + \overline{\rho}\dot{S}^u_{Fu} + \overline{\dot{\omega}}^u_{Fu} - \overline{\dot{\omega}}^{u\to b}_{Fu} \quad (2)$$

Table 6. Calculation domain boundaries [4].

Boundary type	Boundary condition	Values
Piston	Moving mesh	Temperature – 550 K
Axis	Periodic inlet/outlet	Periodic
Cylinder head	Wall	Temperature – 550 K
Compensation volume	Wall	Thermal/adiabatic boundary
Liner	Wall	Temperature – 425 K

Table 7. Models employed in CFD simulation.

Model	Options
Turbulence model	k-ζ-f model
Breakup model	Wave
Turbulent dispersion model	Enable
Wall treatment	Hybrid wall treatment
Wall impingement model	Walljet 1
Heat transfer wall model	Standard wall function
Evaporation model	Dukowicz and multi-component model
Combustion model	CFM
Ignition model	ECFM-3Z
Soot formation and oxidation	Kinetic model
NO_x mechanism	Extended Zeldovich
Chemistry solver	Fire internal chemistry interpreter (CHEMKIN-II)

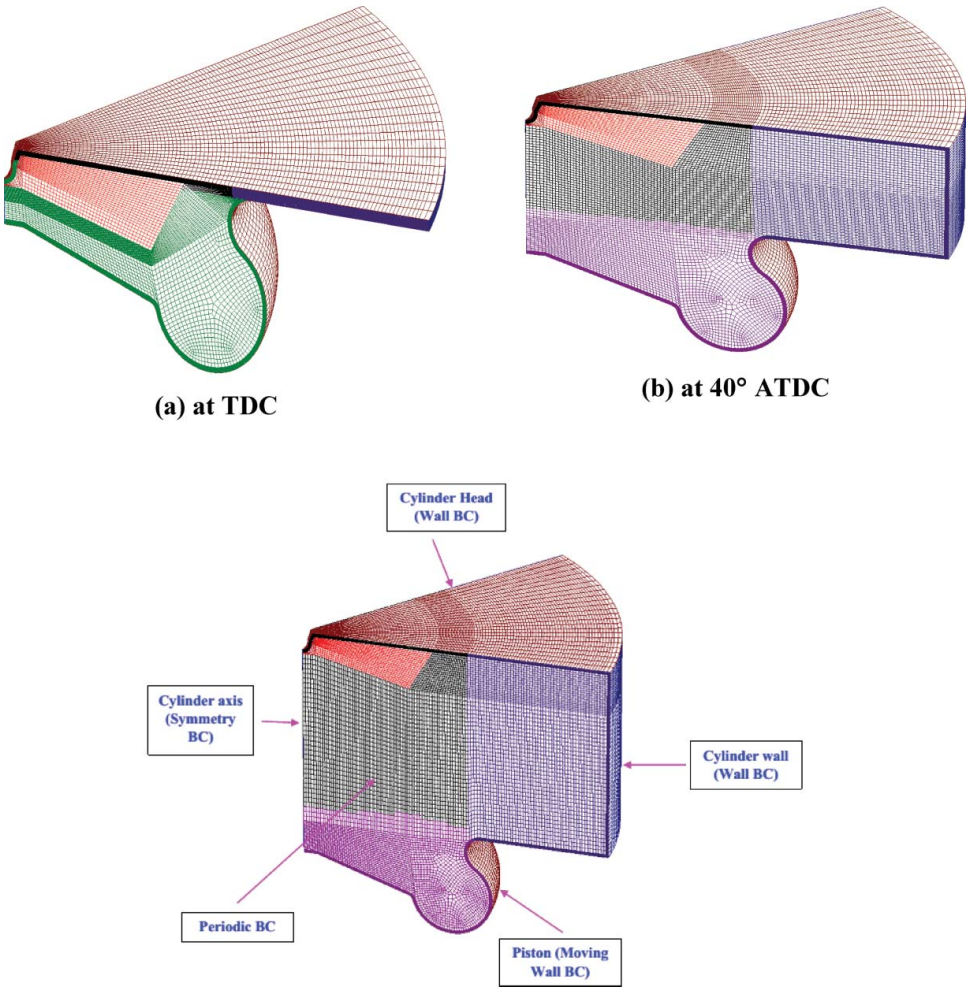

Figure 2. Three-dimensional computational domain. BC: Boundary condition.

$$\frac{\partial(\overline{\rho}\tilde{Y}^b_{Fu})}{\partial t}+\frac{\partial(\overline{\rho}u_i\tilde{Y}^b_{Fu})}{\partial x_i} = \frac{\partial}{\partial x_i}\left(\left(\frac{\mu}{S_c}+\frac{\mu_t}{S_{ct}}\right)\frac{\partial Y^b_{Fu}}{\partial x_i}\right)+\overline{\rho}\dot{S}^b_{Fu}+\overline{\dot{\omega}}^b_{Fu}+\overline{\dot{\omega}}^{u\to b}_{Fu} \quad (3)$$

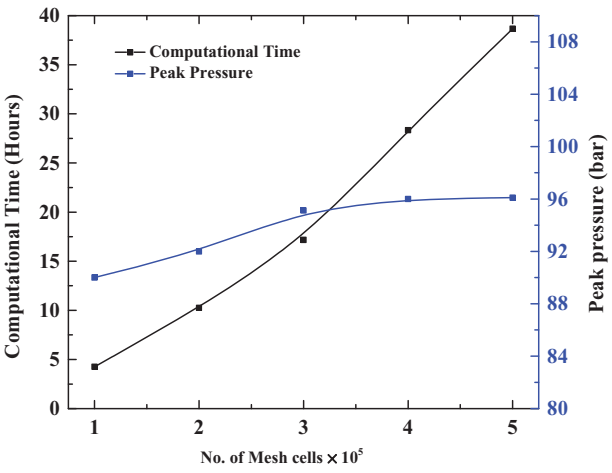

Figure 3. Grid independence study of peak pressure.

The equations for unmixed species, i.e. fuel and air, are:

$$\frac{\partial(\overline{\rho}\tilde{Y}^F_{Fu})}{\partial t}+\frac{\partial(\overline{\rho}u_i\tilde{Y}^F_{Fu})}{\partial x_i}-\frac{\partial}{\partial x_i}\left(\left(\frac{\mu}{S_c}+\frac{\mu_t}{S_{ct}}\right)\frac{\partial Y^F_{Fu}}{\partial x_i}\right) = \overline{\rho}\dot{S}^F_{Fu}+\overline{\rho}\dot{E}^{F\to M}_{Fu} \quad (4)$$

$$\frac{\partial(\overline{\rho}\tilde{Y}^A_{O_2})}{\partial t}+\frac{\partial(\overline{\rho}u_i\tilde{Y}^A_{O_2})}{\partial x_i}-\frac{\partial}{\partial x_i}\left(\left(\frac{\mu}{S_c}+\frac{\mu_t}{S_{ct}}\right)\frac{\partial Y^A_{O_2}}{\partial x_i}\right) = \overline{\rho}\dot{E}^{A\to M}_{O_2} \quad (5)$$

The amount of mixing is computed with a characteristic time scale based on the k-ε model:

$$\overline{\dot{E}}^{F\to M}_{Fu} = -\frac{1}{\tau_m}\tilde{Y}^F_{Fu}\left(1-\tilde{Y}^F_{Fu}\frac{\overline{\rho}M^M}{\overline{\rho}^u|uM_{Fu}}\right) \quad (6)$$

$$\overline{\dot{E}}^{A\to M}_{O_2} = -\frac{1}{\tau_m}\tilde{Y}^A_{O_2}\left(1-\frac{\tilde{Y}^A_{O_2}}{\tilde{Y}^\infty_{O_2}}\frac{\overline{\rho}M^M}{\overline{\rho}^u|uM_{air+EGR}}\right) \quad (7)$$

where τ_m is the mixing time, defined as:

$$\tau_m^{-1} = \frac{\varepsilon}{k} \quad (8)$$

The oxygen mass fraction in unmixed air is computed as follows:

$$\bar{Y}_{O_2}^{\infty} = \frac{\bar{Y}_{TO_2}}{1 - \bar{Y}_{TFu}} \quad (9)$$

Pollutant model

The transport equation model for nitrogen monoxide is given by:

$$\frac{\partial(\bar{\rho}\bar{Y}_{NO})}{\partial t} + \frac{\partial(\bar{u}_i\bar{\rho}\bar{Y}_{NO})}{\partial x_i} = \frac{\partial}{\partial x_i}\left(\bar{\rho}D_t\frac{\partial \bar{Y}_{NO}}{\partial x_i}\right) + \bar{S}_{NO} \quad (10)$$

The term $\bar{S}_{NO}$ is the source term for NO formation in the equation.

$$\bar{S}_{NO} = M_{NO}\left(\frac{dc_{NO\ thermal}}{dt} + \frac{dc_{NO\ prompt}}{dt}\right) \quad (11)$$

The transport equation model for formation of the mass fraction ϕ_s is given by:

$$\frac{\partial}{\partial t}(\bar{\rho}\bar{\phi}_s) + \frac{\partial}{\partial x_j}(\bar{\rho}\bar{u}_j\bar{\phi}_s) = \frac{\partial}{\partial x_j}\left(\frac{\mu_{eff}}{\sigma_s}\frac{\partial \bar{\phi}_s}{\partial x_j}\right) + S_{\varphi_s} \quad (12)$$

The soot formation rate is defined as:

$$S_{\varphi_s} = S_n + S_g + S_{O_2} \quad (13)$$

where S_n = Soot nucleation, S_g= Soot growth and S_{O_2}= Soot oxidation.

Results and discussion

In this section, results of the experimental and numerical (CFD) studies on a CRDI engine are presented. Results were obtained for n-butanol–diesel blends for various EGR rates at different injection timings.

Optimum injection timing for butanol–diesel blends

An experimental result on the effect of injection timing and n-butanol–diesel blends on Brake thermal efficiency (BTE) is presented in Figure 4. The results show that there is a significant increase in BTE for all butanol–diesel blends compared to Bu0. This can be attributed to the promptly premixed combustion part possessed by butanol blends, enhanced mixing during ignition delay, and oxygen enrichment leading to leaner combustion (Hulwan et al. [20]). The enhancement of diffusive combustion is obtained due to oxygen-enriched blends, and hence the total combustion duration is shortened. The increase in BTE with butanol blends is also ascribed to its higher burning velocity of 45 cm/s [21] as compared to 33 cm/s for diesel [22]. The BTE is increased by ~4.5, 6 and 8% for Bu10, Bu20 and Bu30, respectively, compared to Bu0. Based on

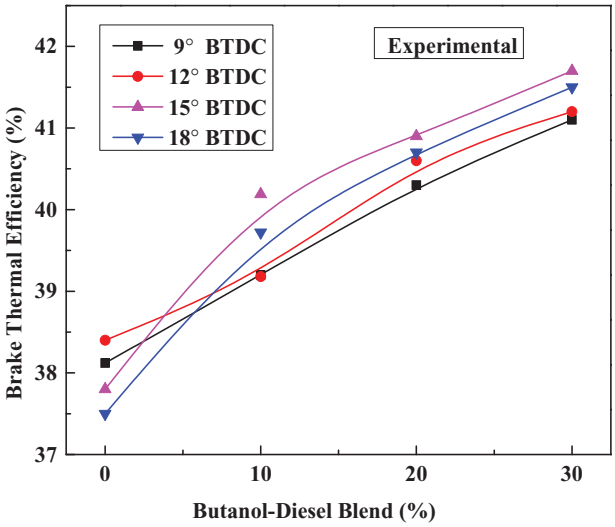

Figure 4. Variation of brake thermal efficiency versus injection timing.

BTE, optimum injection timings are obtained at 12° BTDC for Bu0 and 15° BTDC (common injection timing) for Bu10, Bu20 and Bu30.

To compare the performance and emissions at common injection timing for blends and neat diesel is not justified. Hence, the brake thermal efficiency is presented for optimum injection timings (i.e. 12° BTDC for neat diesel and 15° BTDC for blends) obtained from Figure 4. The effect of EGR rates and n-butanol–diesel blends on BTE is depicted in Figure 5. It is observed that with an increase in the EGR rate, BTE is decreased by approximately 1% for neat diesel (Bu0). The reduction in BTE is due to displacement of intake oxygen (dilution effect), endothermic dissociation of CO_2 and H_2O, and an increase in the heat capacity of the intake charge (thermal effect), resulting in overall reduction of the in-cylinder temperature.

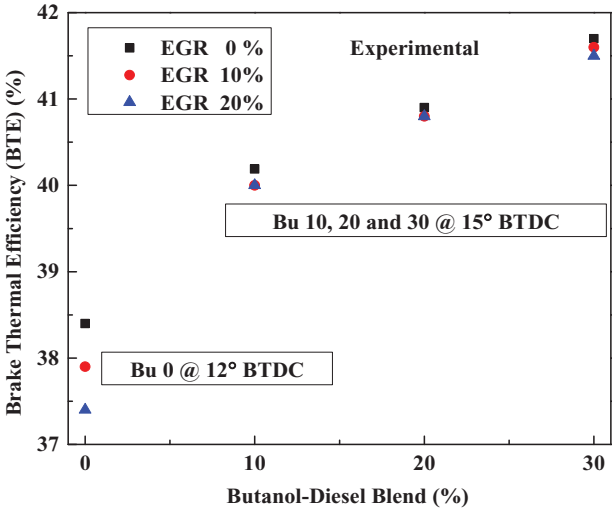

Figure 5. Variation of brake thermal efficiency versus EGR rates.

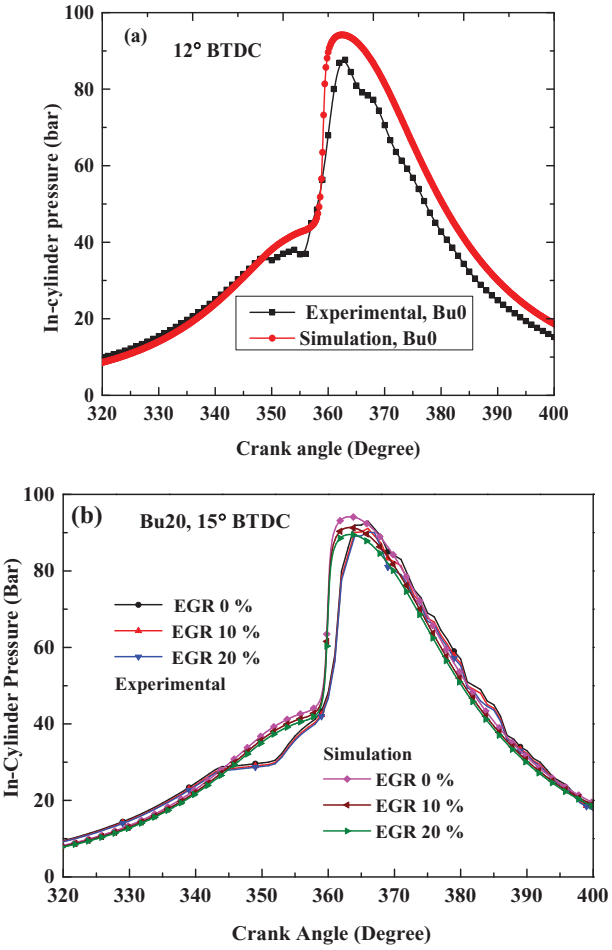

Figure 6. Pressure versus crank angle for different EGR rates: (a) Bu0 at 0% EGR rate, and (b) Bu20 at 0, 10 and 20% EGR rates.

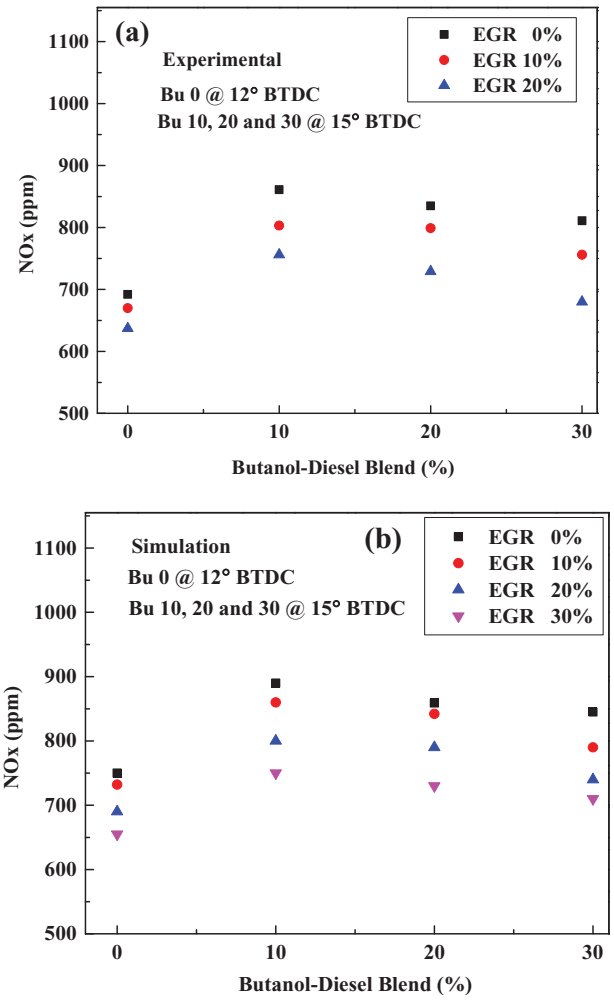

Figure 7. Effect of various EGR rates on Nitrogen oxide (NO) emissions for various butanol–diesel blends: (a) experimental and (b) simulation.

Effect of EGR rate on in-cylinder pressure (validation)

In the present investigation, the engine simulation software AVL-FIRE is coupled with CHEMKIN-II for simulating the in-cylinder combustion and tailpipe emission mechanism with detailed reaction mechanisms. The simulation is validated for pressure versus crank angle from the experimental results obtained from the authors' laboratory for conditions listed in Table 2. Comparisons between experimental and simulation results for Bu0 at 0% EGR, and Bu20 at 0, 10 and 20% EGR, are shown in Figure 3. For all cases, CFD results show good agreement with the experimental data. Hence, this CFD model can be extended for further parametric study.

Effect of various EGR rates on NO_x emission for different butanol–diesel blends

Figure 7(a,b) shows experimental and simulation results of NO_x emission during combustion for various n-butanol–diesel blends at different EGR rates (experimentally: 0, 10 and 20%; simulation: 0, 10, 20 and 30%). Results show that NO emission is reduced with butanol–diesel blends, which occurs due to high latent heat of vaporization of n-butanol resulting in lower in-cylinder temperature compared to diesel. Further increase in EGR rates leads to a decrease in overall in-cylinder temperature due to dilution, thermal and chemical effects. Hence, NO emission is reduced drastically.

NO formation is highly dependent on the in-cylinder temperature, presence of oxygen and available time. High activation energy is required to break the N_2 triple bond; NO formation is significant at very high temperatures. To incorporate this reaction, the Extended Zeldovich Model is used in CFD simulation. Results presented in Figure 7(b) show similar trends compared to the experimental results, which approves the selection of the NO_x model for simulation.

Effects of various EGR rates on CO emission for different butanol–diesel blends

Figure 8(a,b) shows CO emission during combustion for various n-butanol–diesel blends at different EGR

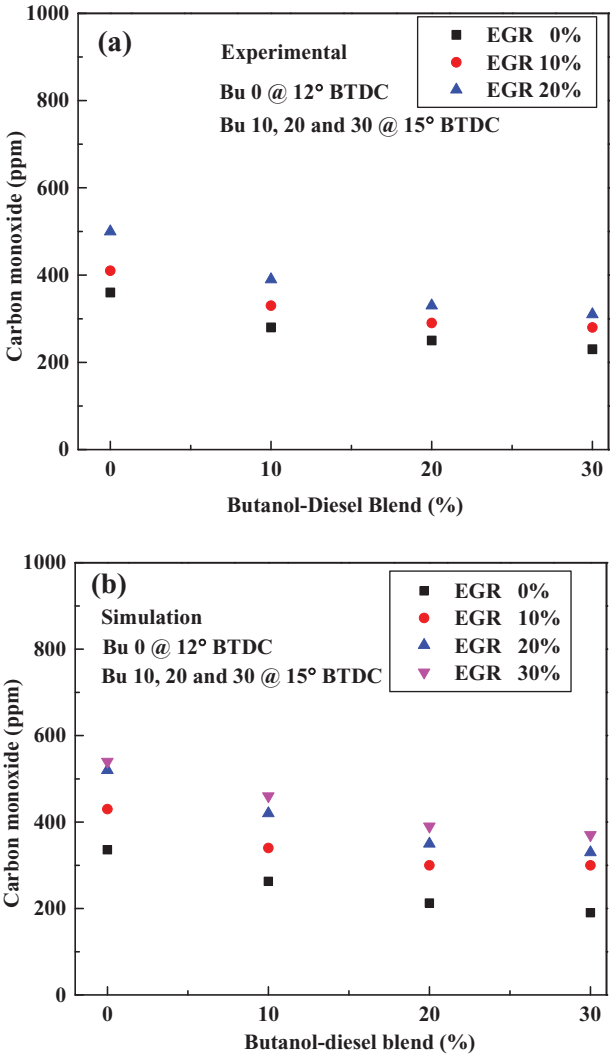

Figure 8. Effect of various EGR rates on CO emissions for various butanol–diesel blends: (a) experimental and (b) Simulation.

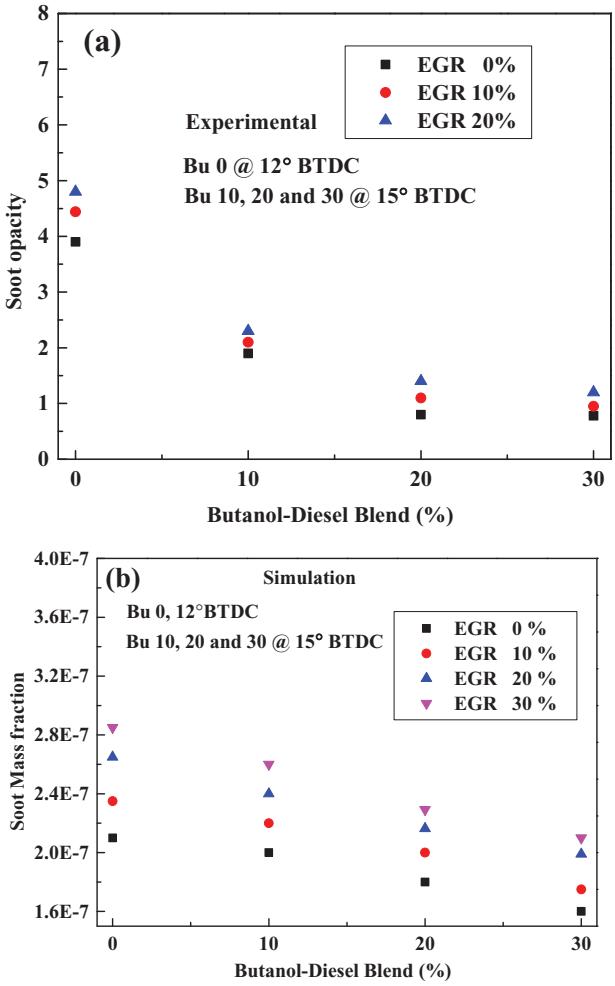

Figure 9. Effect of various EGR rates on soot emissions for various butanol–diesel blends: (a) experimental and (b) simulation.

rates experimentally (0, 10 and 20%) and by simulation (0, 10, 20 and 30%), respectively.

During combustion in the engine, CO formation is an intermediate step. In a later phase with the help of OH radicals, in the presence of oxygen inside the cylinder, oxidation takes place and CO_2 is formed at temperatures above 1200 K. In unoxygenated regions, the oxidation of CO stops due to improper mixing of fuel and air. With an increase in EGR rate, the charge is diluted and more CO formation occurs. It is interesting to know that CO formation is lower for n-butanol–diesel blends with EGR rates compared to neat diesel. From the experimental results it is observed that CO emission for Bu30 (15° BTDC) is decreased by 36, 31 and 38% for 0, 10 and 20% EGR rates, respectively, compared to Bu0 (12° BTDC). The oxygen content of butanol is higher than that of diesel, which causes conversion of CO in fuel-rich regions into CO_2. A similar trend is observed in the simulation studies.

Effect of various EGR rates on soot emission for different butanol–diesel blends

Figure 9(a,b) shows soot emission during combustion for various n-butanol–diesel blends at different EGR rates experimentally (0, 10 and 20%), and by simulation (0, 10, 20 and 30%), respectively. The particulate matter (PM) is basically composed of soot and accounts for the smoke. The formation of opaque smoke ensues under the air deficit conditions which locally exist in the engine cylinder, and increases as the air/fuel ratio declines. Increasing butanol content in the blends results in the reduction of soot due to a higher oxygen/carbon ratio.

From the simulation results it is observed that soot emission for Bu30 (15° BTDC) is decreased by 23, 25, 24 and 26% for 0, 10, 20 and 30% EGR rates, respectively, compared to Bu0 (12° BTDC). The presence of atomic oxygen bonds in butanol fulfills progressive chemical control over soot formation. The smoke meter used for the present experimental studies measures soot opacity rather than the soot mass fraction. The local equivalence ratio is the key parameter for

soot formation. Soot gets oxidized in contact with oxygen and water at elevated temperature. To incorporate soot formation in the CFD simulation, a kinetic soot model is employed. CFD results are obtained for the soot mass fraction, and a similar trend compared to the experimental results is observed.

Conclusion

Experimental and CFD analyses of a four-stroke CRDI engine fuelled with n-butanol–diesel blends for various EGR rates were carried out. The following inferences are made based on the obtained results:

- With the help of the experimental results, an appropriate CFD model to capture the effect of butanol–diesel blends and EGR in a CRDI engine is established.
- Optimum injection timing for Bu0 is obtained at 12° BTDC, while for Bu10, Bu20 and Bu30 it occurs at a common injection timing of 15° BTDC.
- Brake thermal efficiency is decreased by approximately 1% with EGR rate for neat diesel and insignificant effects on biobutanol-blends.
- NO_X emission is reduced with butanol–diesel blends, which occurs due to the high latent heat of vaporization of n-butanol resulting in lower in-cylinder temperature compared to diesel.
- Increase in EGR rates leads to a decrease in overall in-cylinder temperature due to dilution, thermal and chemical effects. Hence, NO emission is reduced drastically.
- Carbon monoxide emission for Bu30 (15° BTDC) is decreased by 36, 31 and 38% for 0, 10 and 20% EGR rates, respectively, compared to Bu0 (12° BTDC).
- Soot emission for Bu30 (15° BTDC) is decreased by 23, 25, 24 and 26% for 0, 10, 20 and 30% EGR rates, respectively, compared to Bu0 (12° BTDC).

Acknowledgements

The authors sincerely acknowledge AVL-AST, Graz, Austria, for granted use of AVL-FIRE simulation software under the university partnership scheme.

Disclosure statement

No potential conflict of interest was reported by the authors.

References

[1] Johnson DT, Taconi KA. The glycerin glut: options for the value added conversion of crude glycerol resulting from biodiesel production. Environ Prog. 2007;26(4):338–348.
[2] Demirbas A. Political, economic and environmental impacts of biofuels: a review. Appl Energ. 2009;86:S108–S117.
[3] Rahmat N, Abdullah AZ, Mohamed AR. Recent progress on innovative and potential technologies for glycerol transformation into fuel additives: a critical review. Renew Sust Energ Rev. 2010;14(3):987–1000.
[4] Lamani VT, Yadav AK, Kumar GN. CFD simulation of a common rail diesel engine with biobutanol–diesel blends for various injection timings.Biofuels and Bioenergy (BICE2016). Springer Proceedings in Energy; 2017. DOI:10.1007/978-3-319-47257-7_14
[5] Zheng M, Li T, Han X. Direct injection of neat n-butanol for enabling clean low temperature combustion in a modern diesel engine. Fuel. 2015;142:28–37.
[6] Heywood, JB. Internal combustion engine fundamentals. Vol. 930. New York: Mcgraw-hill; 1988.
[7] Pundir BP. Engine emissions: pollutant formation and advances in control technology. New Delhi: Narosa Publishing House; 2007.
[8] Zhu Y, Chen Z, Liu J. Emission, efficiency, and influence in a diesel n-butanol dual-injection engine. Energ Convers Manage. 2014;87:385–391.
[9] Rakopoulos DC, Rakopoulos CD, Hountalas, DT, et al. Investigation of the performance and emissions of bus engine operating on butanol–diesel fuel blends. Fuel. 2010a;89(10):2781–2790.
[10] Rakopoulos DC, Rakopoulos CD, Giakoumis EG, et al. Effects of butanol–diesel fuel blends on the performance and emissions of a high-speed DI diesel engine. Energ Convers Manage. 2010b;51(10):1989–1997.
[11] Lujaji F, Kristof L, Bereczky, A, et al. Experimental investigation of fuel properties, engine performance, combustion and emissions of blends containing croton oil, butanol, and diesel on a CI engine. Fuel. 2011;90(2):505–510.
[12] Dogan O. The influence of n-butanol–diesel fuel blends utilization on a small diesel engine performance and emissions. Fuel. 2011;90(7):2467–2472.
[13] Atmanli A, Ileri E, Yüksel B. Experimental investigation of engine performance and exhaust emissions of a diesel engine fueled with diesel–n–butanol–vegetable oil blends. Energ Conver Manage. 2014;81:312–321.
[14] Valentino G, Corcione FE, Iannuzzi SE, et al. Experimental study on performance and emissions of a high speed diesel engine fuelled with n-butanol diesel blends under premixed low temperature combustion. Fuel. 2012;92(1):295–307.
[15] Chen Z, Wu Z, Liu J, et al. Combustion and emissions characteristics of high n-butanol–diesel ratio blend in a heavy-duty diesel engine and EGR impact'. Energ Conver Manage. 2014;78:787–795.
[16] Yao M, Wang H, Zheng Z, et al. Experimental study of n-butanol additive and multi-injection on HD diesel engine performance and emissions. Fuel. 2010;89(9):2191–2201.
[17] Kumar BR, Saravanan S. Effects of iso-butanol/diesel and n-pentanol-diesel blends on performance and emissions of a DI diesel engine under premixed LTC (low temperature combustion) mode. Fuel. 2016;170:49–59.
[18] FIRE v2011 Manuals. Graz, Austria, AVL LIST GmbH; 2011.
[19] Colin O, Benkenida A. The 3-zones extended coherent flame model (ECFM3Z) for computing premixed/diffusion combustion'. Oil Gas Sci Technol. 2004;59(6): 593–609.
[20] Hulwan DB, Joshi SV. Performance, emission and combustion characteristic of a multicylinder DI diesel engine running on diesel–ethanol–biodiesel blends of high ethanol content. Appl Energ. 2011;88:5042–5055.

[21] Sarathy SM, Thomson MJ, Togbe CP, et al. An experimental and kinetic modeling study of n-butanol combustion. Combust Flame. 2009;156(4):852–864.

[22] Sayin C. Engine performance and exhaust gas emissions of methanol and ethanol–diesel blends. Fuel. 2010;89 (11):3410–3415.